13th World Conference on Earthquake Engineering
Vancouver, B.C., Canada
August 1-6, 2004
Paper No. 2978

SEISMIC RELIABILITY ASSESSMENT OF A BRIDGE GROUND SYSTEM

Yuyi ZHANG[1], Gabriel ACERO[1], Joel CONTE[1], Zhaohui YANG[1] and Ahmed ELGAMAL[1]

SUMMARY

Performance-based earthquake engineering (PBEE) is emerging as the next-generation design and evaluation framework under which new and existing structures will be analyzed for seismic adequacy. Various analytical approaches to PBEE are in development [1]. The PBEE methodology developed by the Pacific Earthquake Engineering Research (PEER) Center, headquartered at the University of California, Berkeley, is being exercised and illustrated on real, existing facilities (buildings, bridges, network of highway bridges, campus of buildings) called testbeds. This paper presents the application of the PEER PBEE methodology to one of the six PEER testbeds, namely the Humboldt Bay Middle Channel (HBMC) Bridge, one of three bridges that cross Humboldt Bay, near Eureka in northern California. It is a 330 meter long, nine-span composite structure with precast and prestressed concrete I-girders with cast-in-place concrete slabs, fairly representative of older AASHTO-Caltrans girder bridges with moderate traffic loads. It is supported on eight pile groups in soils potentially vulnerable to liquefaction during an earthquake, which could induce lateral spreading and permanent soil deformations. This bridge testbed is analyzed as a nonlinear structure-foundation-soil system.

This paper focuses on the several analytical steps of the PEER PBEE methodology to assess the seismic reliability of the HBMC Bridge. This methodology integrates probabilistic seismic hazard analysis for the bridge site, advanced computational modeling of the bridge-foundation-soil system, probabilistic seismic demand analysis, probabilistic capacity (or fragility) analysis, and reliability analysis. The earthquake response of the bridge ground system is simulated using a two-dimensional, advanced nonlinear finite element model of the structure-foundation-soil system developed in OpenSees, the new PEER software framework for advanced finite element modeling and seismic response simulation of structural and geotechnical systems. Several potential failure mechanisms are considered such as flexural failure of bridge piers, failure of shear key(s), and unseating. For each failure mechanism, several limit-states or damage-states measuring the stage of formation of the failure mechanism are considered. The seismic reliability against these system-level limit-states is expressed in terms of mean annual frequency (Poisson rate) of exceeding these limit-states or, alternatively, the return period of these limit-states. The paper presents selective results illustrating the various steps of the PEER PBEE methodology as well as their integration.

[1] Department of Structural Engineering, University of California, San Diego, 9500 Gilman Drive, La Jolla, CA 92093-0085 USA, E-mails: jpconte@ucsd.edu, elgamal@ucsd.edu

INTRODUCTION

The Pacific Earthquake Engineering Research (PEER) Center, funded by the U.S. National Science Foundation, is developing a performance-based earthquake engineering (PBEE) methodology for assessment of existing and design of new civil structures such as buildings and bridges. The Humboldt Bay Middle Channel (HBMC) Bridge, near Eureka in northern California, was selected by PEER as one of its six testbed structures [1] to foster the development of and exercise the PEER PBEE methodology for systems with real-world complexities. This bridge structure (Fig. 1) is a 330 meter long, 9-span composite structure with four precast, prestressed concrete I-girders and cast-in-place concrete slabs. For convenience purposes, the piers (or single column bents) are numbered # 1 to 8 from the left (South-East) to the right (North-West). Piers # 3, 4, 5, 6 and 7 are supported on five 54-inch diameter driven precast, prestressed concrete piles, while Piers # 1, 2, 8 and the abutments are founded on sixteen (4 rows of 4) 14-inch driven precast, prestressed concrete square piles. The superstructure is continuous over Piers # 1, 2, 4, 5, 7 and 8. There are expansion joints at the abutments and on top of Piers # 3 and 6. At these expansion joints, there are shear keys with gaps on both sides, while at the continuous joints, a shear key with #4 dowel connects the superstructure to the pier (i.e., shear key without gap). Thus the bridge is separated into three substructures interconnected at the two interior expansion joints. The river channel has an average slope from the banks to the center of about 7% (4 degrees). The foundation soil is composed mainly of dense fine-to-medium sand (SP/SM), organic silt (OL), and stiff clay layers (Fig. 5). In addition, thin layers of loose and soft clay (OL/SM) are located near the ground surface. This site is perceived to be vulnerable to strong ground shaking. Soil liquefaction, approach fill settlement and lateral spreading are issues of interest in this study.

Fig. 1: Humboldt Bay Middle Channel Bridge (Courtesy of Caltrans)

The HBMC Bridge was designed in 1968 and built in 1971 and has been the object of two Caltrans seismic retrofit efforts, the first one completed in 1995, and the second one scheduled for 2004. The objectives of the first retrofit effort were to mitigate the potential for unseating and diaphragm damage (through seat extenders at abutments, as well as pipe seat extenders, end diaphragm retrofit and cable restrainers at interior expansion joints) and to strengthen the shear keys at the interior expansion joints. The second retrofit is planned to strengthen the piers, pile caps, and pile groups. It is an interesting bridge because it is fairly representative of older AASHTO-Caltrans girder bridges with moderate traffic loads (average daily traffic of 4,600 to 15,800 in 1992), designed before ductile detailing was common.

PEER PBEE METHODOLOGY

The major objective of this study is to apply PEER analytical tools and methodologies to evaluate the seismic performance of the HBMC Bridge in probabilistic terms (i.e., compute annual probability of exceeding specific damage limit-states). Following the PEER framework [1, 2], the formidable task of

assessing probabilistically potential bridge damage-states is broken down into four sub-tasks according to the Total Probability Theorem of applied probability theory. These four sub-tasks are (1) Probabilistic Seismic Hazard Analysis, (2) Probabilistic Seismic Demand Hazard Analysis, (3) Probabilistic Seismic Capacity Analysis also called Fragility Analysis, and (4) Seismic Reliability Analysis. These four analytical steps of the PEER PBEE framework are summarized below.

(1) Probabilistic Seismic Hazard Analysis (PSHA)

The objective of PSHA is to compute for a given site the annual probability of exceeding any particular value of a specified ground motion intensity measure (*IM*). The latter is usually taken as the peak ground acceleration or the 5% damped elastic spectral acceleration at a specified period of vibration T, $S_a(T, \xi = 5\%)$. The mean annual rate $\lambda_{IM}(z)$ (or Poisson rate) of exceeding a particular threshold value, z, of a ground motion *IM* is calculated according to the Total Probability Theorem as [3]

$$\lambda_{IM}(z) = \sum_{i=1}^{N_{flt}} \lambda_i \cdot \int_{R_i} \int_{M_i} P\left[IM > z \middle| m, r \right] \cdot f_{M_i}(m) \cdot f_{R_i}(r) \cdot dm \cdot dr \quad (1)$$

where N_{flt} = number of causative faults; λ_i = mean annual rate of occurrence of earthquakes with magnitudes greater than a lower-bound threshold value, m_0, on fault (or seismic source) i. The functions $f_{M_i}(m)$ and $f_{R_i}(r)$ denote the probability density functions (PDF) for magnitude (M_i), and site-to-source distance (R_i), respectively, given the occurrence of an earthquake on fault i. The variables M_i and R_i are assumed to be statistically independent. The conditional probability of *IM* exceeding the threshold value z given $M_i = m$ and $R_i = r$ corresponds to one minus the cumulative distribution function (CDF) of the *IM* attenuation (or predictive relationship of *IM* given seismological variables *M* and *R*) [4, 5]. The simple summation over N_{flt} sources in Eq. (1) assumes statistical independence of earthquake occurrences on different faults (or seismic sources).

By assuming that the random events defined by *IM* exceeding a threshold *value* z at the subject site follow the Poisson random occurrence model, the mean annual rate $\lambda_{IM}(z)$ can be converted into a probability of exceedance, $P[IM_\tau > z]$, during an exposure time τ (in years) as

$$P[IM_\tau > z] = 1 - e^{-\lambda_{IM}(z) \cdot \tau} \quad (2)$$

If the exposure time is taken as one year (i.e., $\tau = 1$), Eq. (2) reduces to

$$P\left[IM_{year} > z \right] = 1 - e^{-\lambda_{IM}(z)} \quad (3)$$

(2) Probabilistic Seismic Demand Hazard Analysis (PSDHA)

The objective of PSDHA is to compute the mean annual rate, $\lambda_{EDP}(d)$, of a given structural response parameter, called engineering demand parameter (*EDP*) in the PEER framework, exceeding a specified threshold value d. $\lambda_{EDP}(d)$ is obtained by convolving the probability distribution of the subject *EDP* conditioned on the seismological variables *M* and *R* and the ground motion *IM*, $P\left[EDP > z \middle| IM, M, R \right]$, with the seismic hazard, $\lambda_{IM}(z)$, as

$$\lambda_{EDP}(d) = \sum_{i=1}^{N_{flt}} \lambda_i \int_{R_i} \int_{M_i} \int_{IM} P\left[EDP > d \middle| IM, M_i, R_i \right] \cdot f_{IM|M_i,R_i}(im \middle| m, r) \cdot f_{M_i}(m) \cdot f_{R_i}(r) \cdot d(im) \cdot dm \cdot dr \quad (4)$$

where $f_{IM|M_i,R_i}(im|m,r)$ denotes the conditional PDF of *IM* given *M*, *R* and the occurrence of an earthquake along seismic fault (or seismic source) *i*. Assuming that the selected *IM* renders *EDP* conditionally independent of *M* and *R*, given *IM*, i.e.,

$$P\left[EDP > d \middle| IM, M_i, R_i\right] = P\left[EDP > d \middle| IM\right], \tag{5}$$

Eq. (4) simplifies to

$$\lambda_{EDP}(d) = \int_{IM} P\left[EDP > d \middle| IM\right] \cdot \left|d\lambda_{IM}(im)\right| \tag{6}$$

The condition of "conditional independence, given IM", expressed in Eq. (5) is called the "sufficiency condition" by Cornell et al. [6,7].

In this study, a discrete set of specified seismic hazard levels (e.g., 2%, 10%, and 50% probability of exceedance in 50 years) is considered for *IM,* which is defined as the 5% damped elastic spectral acceleration at the fundamental period of the computational model of the bridge ground system described below. For each hazard level, an ensemble of earthquake ground motion time histories is developed based on the PSHA results for the subject site as well as the local geological and seismological conditions. Each ground motion record of the ensemble is then scaled to match the IM at the hazard level corresponding to the ensemble. For each selected hazard level, the computational model of the bridge ground system is subjected to each sample of the ensemble of ground motion time histories. The resulting ensembles of *EDP's* needed in the probabilistic bridge performance analysis are analyzed statistically to estimate their probability distribution conditional on *IM*, or more specifically

$$P\left[EDP > z \middle| IM = im\right] = \int_{z}^{\infty} f_{EDP|IM}(x|im) \cdot dx \tag{7}$$

where $f_{EDP|IM}(x|IM)$ denotes the conditional PDF of a specified *EDP* conditioned on the ground motion intensity measure, *IM*.

(3) Probabilistic Seismic Capacity Analysis (PSCA, also called Fragility Analysis)

The objective of PSCA is to compute the probability that a structure or structural component exceeds a specified physical limit-state given the *EDP('s)* associated to this limit-state. The probabilistic assessment of a structural/geotechnical system considers a number of potential limit-states. Typically, these limit-states are characterized by mathematical functions in the form

$$Z_k = R_k - S_k \tag{8}$$

where R_k and S_k denote the resistance or capacity and load effect or demand, respectively, related to the *k*-th limit-state and Z_k is the corresponding safety margin. Z_k is a random variable due to (1) the uncertain capacity term R_k stemming from inherent material, mechanical and geometric properties defining the structure, (2) the modeling uncertainty (also called epistemic uncertainty) associated with the capacity term R_k and the limit-state function as a whole, and (3) the intrinsic variability of the demand as a whole beyond the demand term(s) or *EDP('s)* used in the limit-state function (i.e., missing demand variables effecting the limit-state under consideration). Traditionally, the above sources of uncertainty are modeled and quantified through the probability of exceeding the *k*-th limit-state conditioned on the demand variable S_k, namely

$$P\left[Z_k < 0 \middle| S_k = s\right] \tag{9}$$

The probabilistic analysis involved to evaluate the above conditional probability of limit-state exceedance is traditionally called *fragility analysis*. The only way to assess capacity model uncertainty is to compare

model predictions with real-world observations, either in the field or in the laboratory, and to perform statistical model assessment [8].

(4) Seismic Reliability Analysis (SRA)

The objective of SRA is to compute the mean annual rate, λ_{LS_k}, of exceeding the *k*-th limit-state of a specific structural/geotechnical system. λ_{LS_k} is obtained by convolving the probability of exceeding the *k-th* limit-state conditioned on the demand variable (*EDP*), $P\left[Z_k < 0 \middle| EDP = d\right]$, with the demand hazard, $\lambda_{EDP}(d)$, as

$$\lambda_{LS_k} = \int_{EDP} P\left[Z_k < 0 \middle| EDP = d\right] \cdot \left|d\lambda_{EDP}(d)\right| \tag{10}$$

PROBABILISTIC SEISMIC HAZARD ANALYSIS

Uniform hazard spectra for this site were developed by Somerville and Collins [9] based on comparison of three estimates: the USGS probabilistic seismic hazard maps for rock site (NEHRP B/C) conditions [10], Geomatrix Consultants spectra for rock site conditions [11], and the PG&E spectra for rock site conditions at the nearby Humboldt Bay Power Plant [12]. The USGS spectra were used as a basis for developing rock spectra at the site as they are close to the average of the three estimates. The rock spectra were modified to include near-fault rupture directivity effects using the model of Somerville et al. [13]. The soil spectra were generated from the rock site spectra by multiplying the rock spectra by the ratio of soil to rock spectra for the Abrahamson and Silva ground motion model [4]. Three seismic hazard levels were selected, namely 50%, 10% and 2% probability of exceedance in 50 years. The uniform hazard spectra for these three hazard levels for both rock and soil site conditions at Humboldt Bay are shown in Fig. 2. The seismic hazard curves (in terms of annual probability of exceedance, *PE*) for soil and rock site conditions and for *IM* taken as $S_a\left(T_1 = 1.25sec, \xi = 5\%\right)$ (the 5% damped elastic spectral acceleration at the fundamental period T_1 of the computational model of the bridge ground system) are approximated from three points and are assumed bilinear in the linear scale for *IM* and logarithm scale for *PE* as shown in Fig. 3. The seismic hazard curves in terms of mean annual rate of exceedance, $\lambda_{IM}(z)$, can then be derived from those in terms of the annual probability of exceedance through Eq. (3) (see Fig. 4).

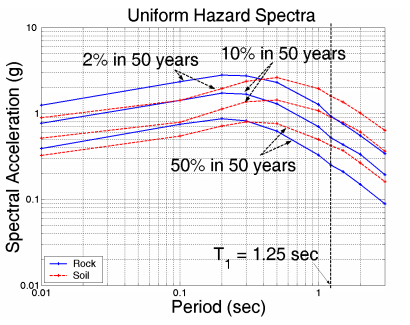

Fig. 2: Uniform Hazard Spectra

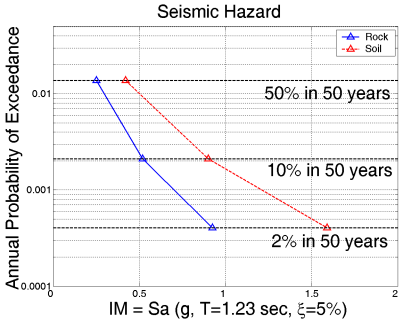

Fig. 3: Seismic Hazard Curves

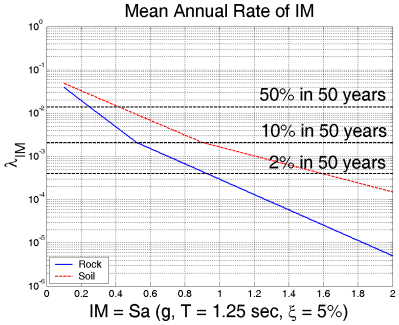

Fig. 4: $\lambda_{IM}(z)$

The deaggregation of the seismic hazard at T_1 = 1.25 sec indicates that [9]: (1) for the 50% in 50 years hazard level, the largest contributions come from magnitude 7 earthquakes within the Gorda Plate, which underlies the site at a depth of 20 km; (2) for the 10% in 50 years hazard level, the largest contributions come from magnitude 7.5 shallow thrust earthquakes on the Little Salmon fault located 9 km south-

southwest of the HBMC Bridge; (3) for the 2% in 50 years hazard level, the largest contributions come from the synchronous occurrence of a large subduction earthquake on the Gorda-North American plate interface and rupture of the Little Salmon fault. A total of 51 ground motion time histories were selected by Somerville and Collins [9] to satisfy to the extent possible the magnitude and distance combinations from the seismic hazard deaggregation. All 22 recordings (17 soil records and 5 rock records) at hazard level 50% in 50 years are from earthquakes in the Cape Mendocino, California region. The recordings at hazard level 10% in 50 years (15 soil records and 4 rock records) are from diverse earthquakes: two from the 1992 Cape Mendocino earthquake, two from the 1978 Tabas, Iran earthquake, and the remaining fifteen from the 1999 Chi-chi, Taiwan earthquake. The 10 recordings (2 soil records and 8 rock records) at hazard level 2% in 50 years originate from large interplate subduction earthquakes: the 1985 Valparaiso, Chile and Michoacan, Mexico earthquakes [9].

COMPUTATIONAL MODEL OF BRIDGE GROUND SYSTEM

A two-dimensional nonlinear finite element model of the HBMC Bridge in its "as-built" condition [14], including the superstructure, abutments, piers, supporting piles, pile caps and soil was developed using OpenSees [15], the new PEER analytical platform for seismic response simulation of structural and geotechnical systems. This model is shown in Fig. 5. This study deals only with the seismic response of the bridge in its longitudinal direction. The response of the bridge in the transversal direction is ignored, to remain within acceptable computational time (i.e., less than 15 hours) per response history analysis. Within each span, the four I-girders are idealized as single equivalent linear elastic beam-column element. Each bridge pier is modeled using a single nonlinear material, fiber beam-column element (with five Gauss-Lobato points along its length) formulated using the flexibility (or force-based) approach based on the exact interpolation of the internal forces [16]. The cross-section of each pier is discretized into concrete and steel fibers as shown in Fig. 6c. The uniaxial Kent-Scott-Park constitutive model (Fig. 6a) with degraded linear unloading & reloading stiffness is used to model the concrete material, while the uniaxial bilinear model (or uniaxial J_2 plasticity model with linear kinematic hardening, Fig. 6b) is used to model the reinforcing steel. The unconfined concrete (outside transverse reinforcement) is characterized by smaller compressive and residual strengths as well as smaller strain ductility than the confined concrete (inside transverse reinforcement). At the base of the eight piers, all the longitudinal reinforcing bars are lap spliced. A macro-element (Fig. 7a) was developed to model the macroscopic behavior of the lap spliced regions. Based on experimental data on lap-spliced columns and the construction drawings of the HBMC Bridge, the length of the lap-spliced regions (= height of macro-element) was taken as 15 times the diameter of the spliced bars. The four horizontal bars and the two vertical bars in the center of this macro-element (denoted by R) are modeled as quasi-rigid beam-column elements. The two vertical components on the sides of the macro-element are modeled as truss elements with an aggregated uniaxial material model made of the following two uniaxial material models in parallel: (1) linear elastic material in series with a gap (denoted by C), and (2) hysteretic material in tension with no strength in compression (denoted by T). As shown in Fig. 7a, the free ends of the two vertical rigid links are connected with two zero-length elements; the vertical zero-length element is made of a uniaxial linear elastic material model in series with a gap (denoted by C), while the horizontal zero-length element is made of a uniaxial linear elastic material model (denoted by S). The horizontal zero-length element transfers the shear force across the element accounting for the small elastic shear deformation across the spliced region. The macro-element for the pier spliced regions was calibrated based on the envelope (skeleton curve) of the moment-rotation behavior of the piers of the HBMC Bridge as predicted by a detailed mechanics-based model of lap spliced columns. Fig. 7b shows the moment-rotation hysteresis loops predicted by the calibrated macro-element subjected to cyclic rotations of increasing amplitudes and keeping the axial load fixed (= axial load of bridge pier under gravity loads alone). The same figure indicates the contributions of the axial load and of the (spliced) rebars to the envelope of the moment-rotation hysteresis loops. In the 2D model of the bridge ground system developed, every out-of-plane row of piles is modeled as a single equivalent/lumped pile with a cross-section identical to the union/sum of the cross-sections of the piles in that row. This

equivalent/lumped pile is then discretized into a number of force-based, fiber beam-column elements (with two Gauss-Lobato points along their length). The shear keys at the abutment joints, interior expansion joints and continuous joints are modeled using zero-length elements with an aggregated uniaxial material model defined by an "elasto-plastic model with gap" and an "elasto-plastic model with hook" configured in parallel. In order to simulate the physical fracture of shear keys, the ultimate deformation of each shear key is specified so that the internal force of the shear key drops to zero when this deformation is reached and remains zero thereafter.

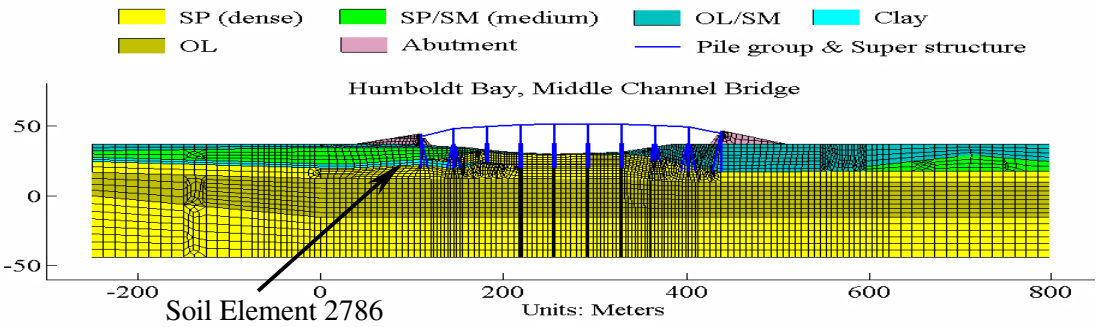

Fig. 5: *OpenSees* Finite Element Model of Humboldt Bay Middle Channel Bridge Ground System (based on blue prints courtesy of Caltrans, mesh constructed using GID software)

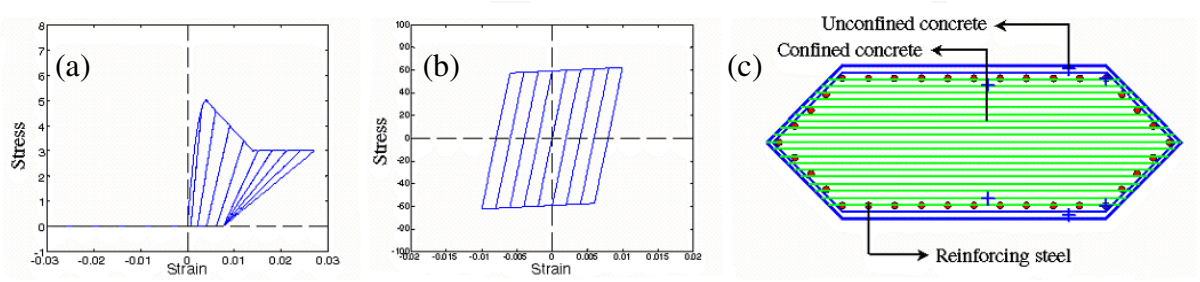

Fig. 6: Uniaxial Stress-Strain Law for (a) Concrete (Kent-Scott-Park model), and (b) Reinforcing Steel (bilinear model with kinematic hardening), and (c) Fiber Discretization of Pier Cross-Section

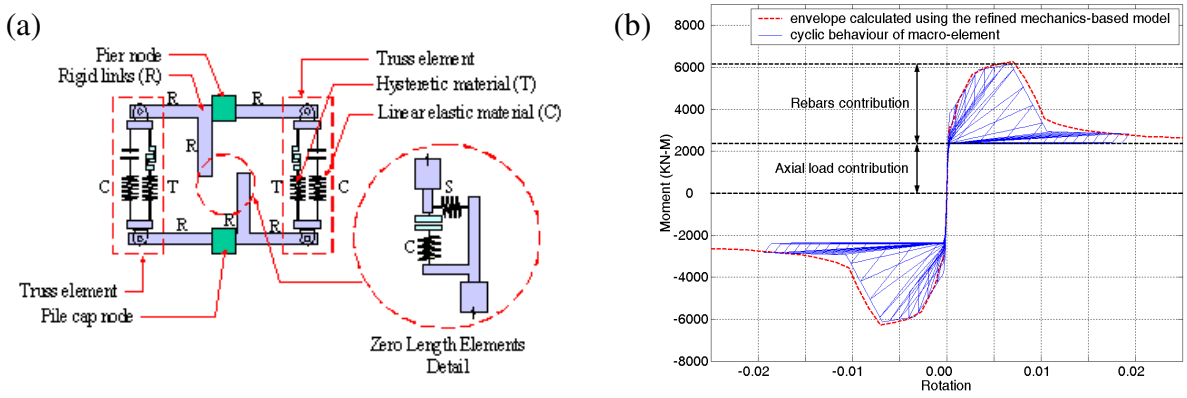

Fig. 7: (a) Macro-Element for Lap Spliced Regions; (b) Cyclic Behavior of Macro-Element

The soil domain is analyzed under the assumption of plane strain condition. It is spatially discretized using four-noded, bilinear, isoparametric finite elements with four integration points each. The materials in the various layers of the soil domain are modeled using an effective-stress multi-yield-surface plasticity model [17]. Liquefaction effects are accounted for by an undrained formulation. The piles are connected to

the surrounding soil domain directly, not accounting for friction effects between soil and piles and gapping between soil and piles near the ground surface for the sake of simplicity.

The lateral and base boundary conditions for the computational soil domain are modeled using a modified Lysmer transmitting/absorbing boundary [18]. A set of horizontal viscous dampers along the soil boundaries is used to implement these transmitting boundaries. Consistent with the assumption of vertical incident shear waves (i.e., 1-D vertical shear wave propagation) and an undamped elastic half-space underlying the computational nonlinear soil domain, the seismic input is defined as equivalent nodal forces, which are proportional to the velocity of the incident seismic wave, applied in the horizontal direction along the base of the computational soil domain. The 51 ground motion time histories developed based on PSHA are free surface motions for both soil and rock site conditions. In the case of rock motions, we assume that the free surface motion represents the rock outcropping motion. In the case of vertically propagating shear waves in a homogeneous, undamped, elastic half-space, the amplitude of the total free surface motion is twice the amplitude of the incident motion at any point in the half-space. Thus, for each of the rock site motions, the incident seismic wave is taken as half the free surface ground motion. For soil motions, the free surface motions are deconvolved iteratively (using equivalent linear soil layer models) using SHAKE [19] following the procedure recommended by Silva [20] to obtain the corresponding incident wave motions at the base of the computational soil domain.

FAILURE MECHANISMS, LIMIT-STATES, AND ASSOCIATED EDP's

As an illustration of the PEER PBEE methodology, the following three potential failure mechanisms are considered herein for the HBMC Bridge: (1) flexural failure in lap spliced region of piers, (2) unconfined shear key(s) failure (with strut-and-tie governing mechanism along diagonal crack pattern), and (3) unseating at the abutments and at the interior expansion joints. Each of these failure mechanisms has been observed in previous earthquakes. For each failure mechanism, five discrete stages of mechanism formation, also called limit-states or damage-states, are considered. These performance-based limit-states are defined as follows [21]: I - cracking, II - yielding, III - formation of the mechanism (at which state the peak capacity is reached), IV - total formation of mechanism, and V - strength degradation (collapse). Each of these limit-states is associated with a repair need from "no repair required" to "replacement of the component" as well as socio-economic implications from "fully operational" to "near collapse". These five limit-states are marked in Fig. 8 on a typical force-deformation response for an unconfined shear key [22] and depicted qualitatively in the form of digital pictures in Fig. 9 [23].

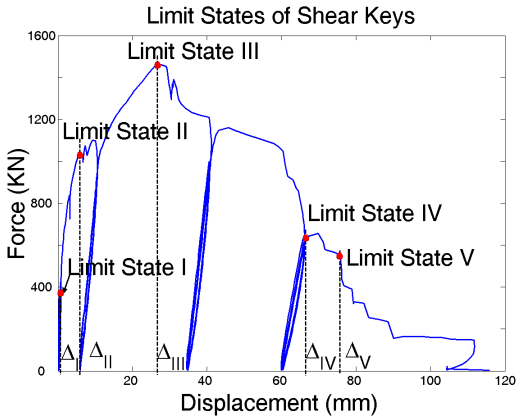

Fig. 8: Typical Force-Deformation Response and Limit-States for Unconfined Shear Key

(a) Limit-state I **(b) Limit-state II** **(c) Limit-state III** **(d) Limit-state IV** **(e) Limit-state V**

Fig. 9: Pictorial Description of Limit-States of Unconfined Shear Key

The maximum lateral (or tangential) drift Δ defined in Fig. 10 for each pier was selected as *EDP* for flexural failure in the lap spliced region of the bridge piers. The five limit-states are marked in Fig. 11 in the moment-lateral drift response for a typical pier of the HBMC Bridge, which was predicted analytically based on refined section analysis and modified material constitutive models/parameters to account for the transfer force mechanism between concrete and rebars, the bond-slip degradation, the length of the yield plateau in the stress-strain law of the spliced reinforcing steel, the length of the spliced region, the strain penetration effect, and the axial load ratio. In this particular case (considering the range of variation of the pier axial load ratio during the earthquake response simulations performed) as illustrated in Fig. 11, it was found that limit-states III, IV and V occur at very close lateral drift values, indicating the brittle nature of this failure mechanism for the HBMC Bridge. Thus, only two limit-states were considered for this failure mechanism, namely limit-state II (yielding) and the joint limit-state III-IV-V (peak capacity and immediate collapse). Simplified mechanistic capacity models show that the shear keys of the HBMC Bridge are characterized by a similar brittle behavior, due to the low amount of reinforcement as well as the short anchorage length specified in the "As Built" configuration of the HBMC Bridge. For the shear key(s) failure mechanism, the maximum deformation across each shear key is selected as an *EDP*. The limit-states I, II, and III for this failure mechanism fall within a very small deformation range. Therefore the five limit-states can be reduced to joint limit-state I-II-III, limit-state IV and limit-state V. Regarding the unseating failure mechanism, only limit-state V (collapse) is considered and the associated *EDP* is taken as the maximum horizontal displacement of the superstructure away from its supports (at abutments and interior expansion joints).

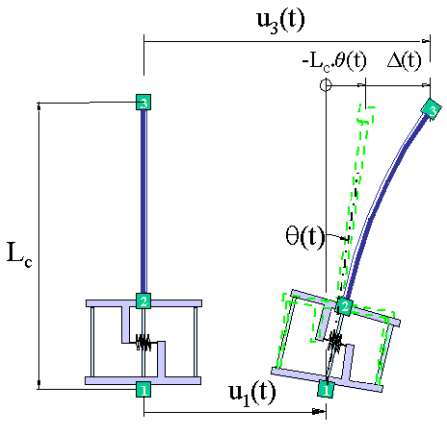

Fig. 10: Definition of Pier Lateral Drift

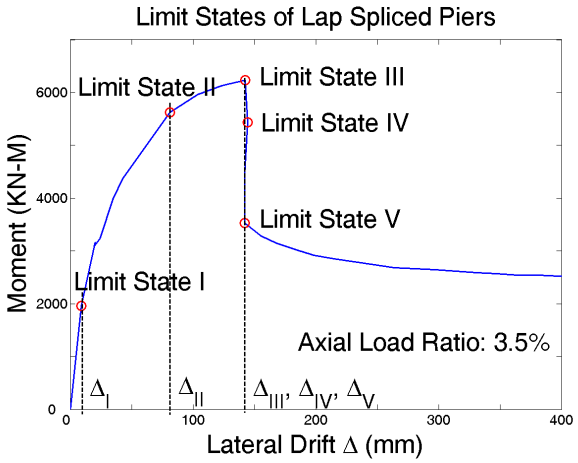

Fig. 11: Limit-States of Lap Spliced Piers

PROBABILISTIC SEISMIC DEMAND ANALYSIS

The computational model of the structure-foundation-soil system is subjected to the 51 ground motion time histories developed based on PSHA. Some typical responses of the soil and the structure at the three hazard levels are displayed in Figs. 12 through 15. It is observed from Figs. 14a and 14b that the pier tops within the same substructure (the bridge is made of three interconnected substructures) undergo the same horizontal motion due to the high axial stiffness of the girders. Fig. 14c shows that one substructure undergoes quite different horizontal motion from the other two after fracture of a connecting shear key. The pier bottoms, however, move progressively and permanently towards the center of the river channel. The permanent deformation of the bridge ground system at the end of an earthquake excitation shown in Fig. 16 (in exaggerated scale) indicates that the embankments slump and move (flow) together with the river banks towards the center of the river channel (as indicated by the arrows) due to soil lateral spreading induced by the build-up of the pore pressure during seismic response.

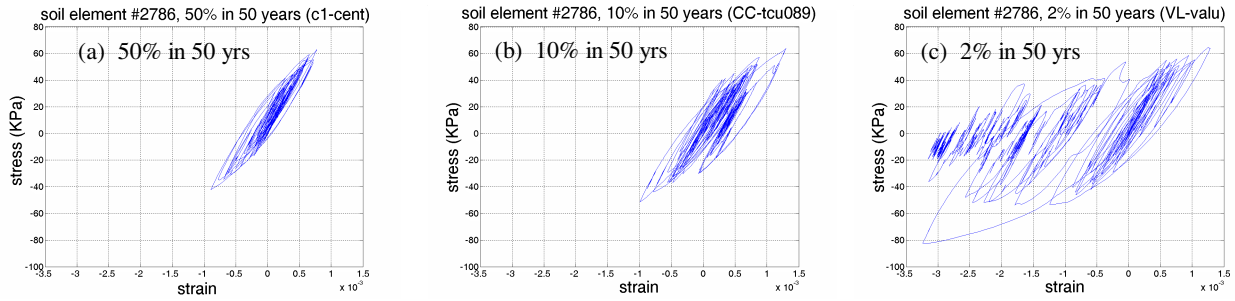

Fig. 12: Shear Stress – Shear Strain Soil Response (see Fig. 5)

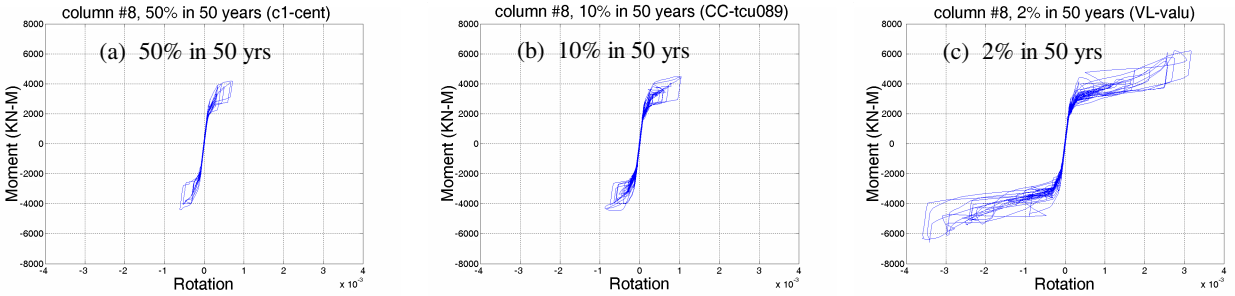

Fig. 13: Moment - Rotation Response of Lap Splice Macro-Element at Base of Pier # 8

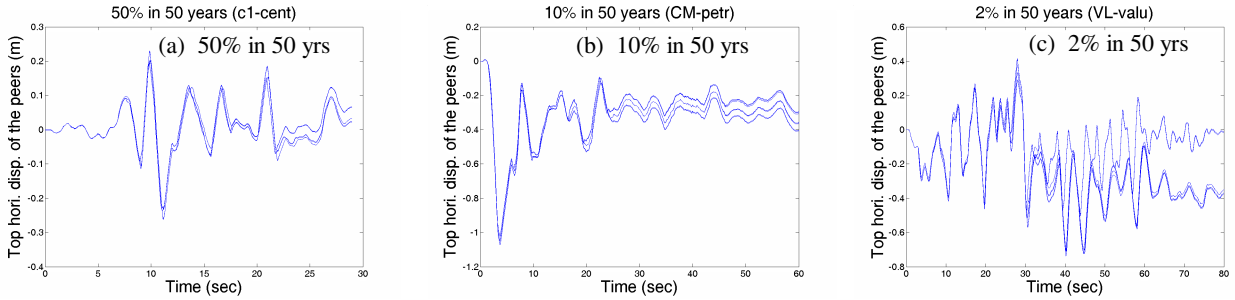

Fig. 14: Top Horizontal Displacement of Piers

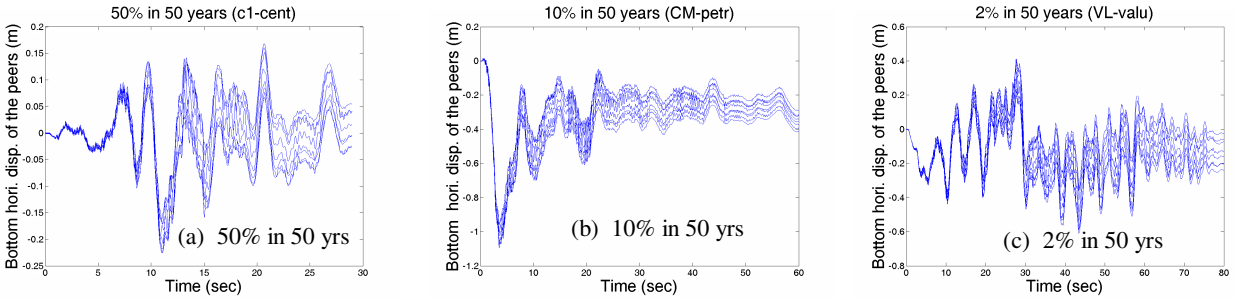

Fig. 15: Bottom Horizontal Displacement of Piers

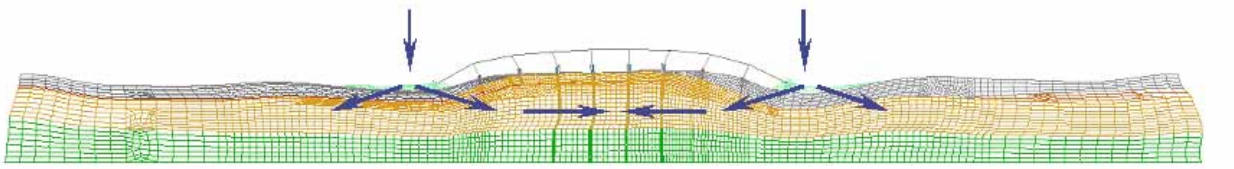

Fig. 16: Permanent Deformation of Bridge Ground System at the End of an Earthquake (exaggerated scale)

The following system-level *EDP's* are used to capture the load effects for the three failure mechanisms considered here (lap-spliced pier failure, shear key failure, and unseating): maximum lateral drift over all bridge piers, maximum shear key deformation at abutment-superstructure joints, maximum shear key deformation at interior expansion joints, maximum shear key deformation at continuous joints, maximum horizontal displacement of the superstructure away from its supports at the abutments, and at the interior expansion joints. Each ensemble of *EDP*'s simulated using OpenSees for a given *IM* is analyzed statistically to estimate the probability distribution of EDP's conditioned on *IM*, i.e., $P\left[EDP > z \mid IM\right]$. The probability distribution of each *EDP* given *IM* is assumed to follow the lognormal probability distribution. The relation between *IM* and the median $\mathrm{EDP} = \exp\left(\lambda_{\mathrm{EDP}}\right)$ of the lognormal distribution of each *EDP* given *IM* is approximated by a function of the form

$$\mathrm{EDP} = \exp\left(\lambda_{\mathrm{EDP}}\right) = a \cdot \mathrm{IM}^{b} \qquad (a, b > 0) \tag{11}$$

The standard deviation ζ of the natural logarithm of each *EDP* condition on *IM* is approximated as

$$\zeta(\mathrm{IM}) = c \cdot \mathrm{IM} \cdot \exp\left(-d \cdot \mathrm{IM}\right) \qquad (c, d > 0) \tag{12}$$

The above relation yields $\zeta = 0$ for $IM = 0$ and for very large *IM*. The *EDP* defined as the maximum pier lateral drift Δ is used here to illustrate the probabilistic demand analysis as shown in Fig. 17. At each hazard (*IM*) level, the peak lateral drift over all eight piers is obtained from each nonlinear time history analysis and the resulting ensemble of *EDP* values is separated into two sub-ensembles according to the local site characterization (i.e., soil site or rock site) of the time history used to define the seismic input. Each sub-ensemble is fitted a lognormal distribution using the least squares method. The fitted lognormal distribution parameters λ and ζ at the three hazard levels are used separately for soil site time histories and rock site time histories to determine (a, b) in Eq. (11) and (c, d) in Eq. (12), respectively, using the least squares method. The seismic demand hazard curve $\lambda_{\mathrm{EDP}}(d)$ shown in Fig. 18. is obtained by convolving the conditional probability of exceedance $\mathrm{P}\left[\mathrm{EDP} > d \mid \mathrm{IM}\right]$ with the seismic hazard curve, $\lambda_{\mathrm{IM}}(z)$, as

$$\begin{aligned}\lambda_{\mathrm{EDP}}(d) = &\int_{\mathrm{IM}} \mathrm{P}\left[\mathrm{EDP} > d \middle| \mathrm{IM}, \mathrm{Rock}\right] \cdot \frac{n_{\mathrm{rock}}(\mathrm{im})}{n_{\mathrm{soil}}(\mathrm{im}) + n_{\mathrm{rock}}(\mathrm{im})} \cdot \left|d\lambda_{\mathrm{IM,Rock}}(\mathrm{im})\right| \\ &+ \int_{\mathrm{IM}} \mathrm{P}\left[\mathrm{EDP} > d \middle| \mathrm{IM}, \mathrm{Soil}\right] \cdot \frac{n_{\mathrm{soil}}(\mathrm{im})}{n_{\mathrm{soil}}(\mathrm{im}) + n_{\mathrm{rock}}(\mathrm{im})} \cdot \left|d\lambda_{\mathrm{IM,Soil}}(\mathrm{im})\right|\end{aligned} \tag{13}$$

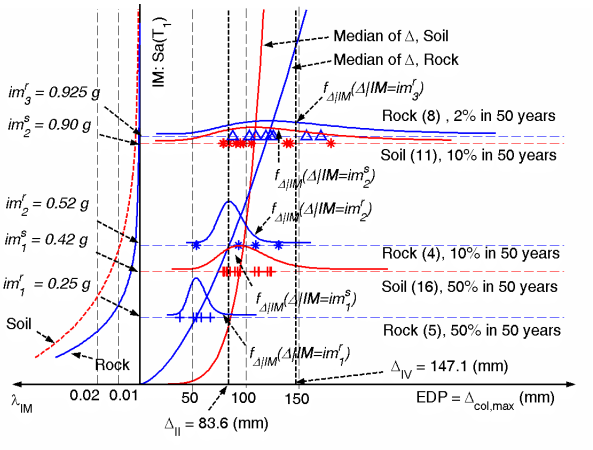

Fig. 17: Response Analysis Conditioned on *IM*

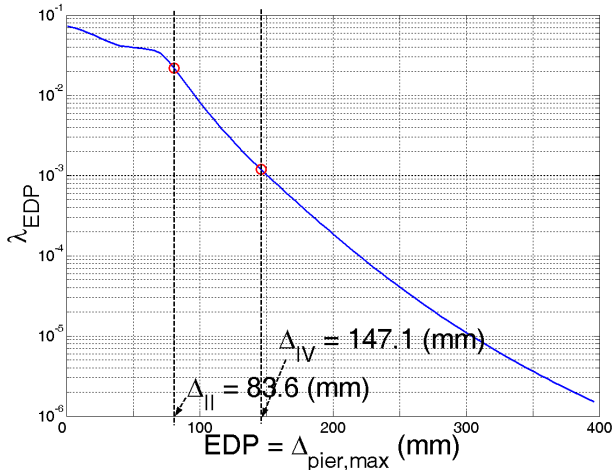

Fig. 18: Demand Hazard Curve for Maximum Pier Lateral Drift at System Level

where $n_{rock}(im)$ and $n_{soil}(im)$ are the number of rock site time histories and soil site time histories, respectively, at the hazard level *IM* = *im*. The seismic demand hazard curves $\lambda_{EDP}(d)$ for the other system-level *EDP's* are computed following the same procedure.

PROBABILISTIC SEISMIC CAPACITY ANALYSIS (FRAGILITY ANALYSIS)

Univariate probabilistic capacity models (or fragility curves) are developed in this study to assess the fragility of the HBMC Bridge in regards to the potential failure mechanisms identified. The fragility function for a limit-state characterizing a given stage of formation of a failure mechanism is defined as the probability of exceeding this limit-state conditioned on the *EDP's* associated with this limit-state (i.e., used to evaluate whether this limit-state has been reached or exceeded). It is assumed herein that a single (scalar) *EDP* is associated to each limit-state of each potential failure mechanism.

The probabilistic capacity models used in this study are based on existing and newly developed deterministic predictive capacity models and experimental data. For each limit-state considered, a set of experimental data was collected from previous tests. For each experimental data point, the experimental (or measured) over calculated (or predicted) capacity ratio is computed. If the predictive capacity model were perfect and in the absence of inherent and modeling uncertainties and measurement noise/errors, these experimental over calculated capacity ratios would all be unity and, therefore, the fragility function would take the form of a step function centered at the unit value. However, in reality, these ratios exhibit a scatter due to imperfect capacity models, missing explanatory variables, and various sources of randomness/uncertainty. In this study, these ratios are approximated by the Normal distribution for each limit-state of each failure mechanism. The fragility curves are obtained by fitting the Normal distribution to the experimental over calculated capacity ratios using the least squares method. The uncertainty of the capacity ratio decreases with increase of the slope of the fragility curve, while the bias of the predictive capacity model is given by the ratio corresponding to a fragility value of 50%. If the bias is unity, then the predictive capacity model is unbiased.

A refined deterministic, mechanistic model, which is more accurate than the widely used model recommended by Priestley et. al. [24], was developed to predict the capacity against each of the five limit-states of pier flexural failure in the lap spliced region. These predicted flexural capacities are functions of the axial load ratio, which varies continually during an earthquake. However, the deformation-based (in terms of pier lateral drift) predicted capacities are not strongly sensitive to the changes in the axial load ratio (0.9%-4.5%) experienced during an earthquake. Therefore, in this study, the predictive capacities (in the denominator of the capacity ratio) are computed at the axial load ratio under gravity loads alone. The experimental data used to develop the fragility curves originate from 10 lap spliced column specimens (4 tested at UCSD [21] and the other 6 tested at UCLA [25]). Each test specimen provides two data points (in the push and pull directions, respectively) for each limit-state. The fragility curves shown in Fig. 19 were thus obtained by fitting a Normal cumulative distribution function (CDF) to the empirical CDF defined by the 20 values of the experimental over calculated capacity ratio.

For the shear key(s) failure mechanism, a predictive capacity model developed at USCD by Megally et al. [23] was adopted. Experimental tests for (unconfined) shear keys are scarce, and the fragility curves shown in Fig. 20 were derived based on the following experimental results: 3 tests by Megally et al. [23] and 2 tests by Bozorgzadeh et al. [22]. Unfortunately, no experimental data is available for the unseating failure mechanism and the fragility curves shown in Fig. 21 were obtained from simple engineering judgement.

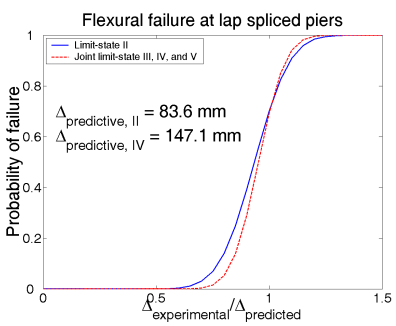

Fig. 19: Fragility Curves for Flexural Failure at Piers

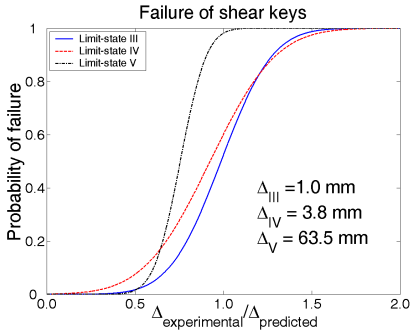

Fig. 20: Fragility Curves for Failure of Shear Keys

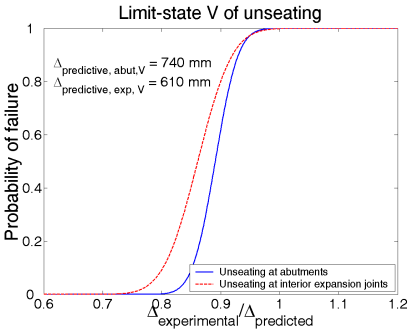

Fig. 21: Fragility Curves for Unseating

SEISMIC RELIABLITY ANALYSIS

For the three potential failure mechanisms considered, the mean annual rate of exceeding the *k*-th limit-state, λ_{LS_k}, is obtained by convolving the corresponding fragility curve with the demand hazard curve, $\lambda_{EDP}(d)$, as expressed in Eq. (10). The mean annual rates of limit-state exceedance calculated are summarized in Table 1.

Table 1: Probabilistic Performance Assessment Results

Failure Mechanism	Limit-State	Mean Annual Rate of Exceedance	Mean Return Period T (years)
Flexural failure at lap spliced piers	II: Yielding	0.025	40
	IV: Full development of mechanism	0.0018	556
Failure of shear keys at abutments	III: Initiation of mechanism	0.065	15
	IV: Full development of mechanism	0.05	20
	V: Strength degradation	0.0017	588
Failure of shear keys at continuous joints	III: Initiation of mechanism	0.05	20
	IV: Full development of mechanism	0.026	39
	V: Strength degradation	1.6×10^{-4}	6,416
Failure of shear keys at interior expansion joints	III: Initiation of mechanism	0.068	15
	IV: Full development of mechanism	0.054	19
	V: Strength degradation	0.0066	152
Unseating at abutments		1.5×10^{-4}	6,830
Unseating at interior expansion joints		7.1×10^{-5}	14,150

The probabilistic performance assessment results obtained in this study reveal that, among the potential failure mechanisms considered, the most critical damage-states are the initiation (return period from 15 to 20 years) and full development (return period from 19 to 39 years) limit-states of the shear keys failure mechanism, especially at the abutments and at the interior expansion joints. The yielding limit-state of the pier lap splice flexural failure mechanism is also critical with a return period of 40 years. Thus, the pier flexural failure mechanism is the most critical mechanism causing an overall collapse of the bridge. It is also observed from Table 1 that unseating is a very unlikely failure mechanism of the bridge. This is most likely due to the typical deformation pattern (see Fig. 5) of the bridge ground system when subjected to seismic excitation. Due to lateral soil spreading, the superstructure of the bridge is in an overall

compressive mode, increasing the safety of the bridge against unseating. The above results mostly justify the retrofit efforts of Caltrans.

CONCLUSIONS

This paper presents the application of the newly developed performance-based earthquake engineering (PBEE) methodology of the Pacific Earthquake Engineering Research (PEER) Center to the Humboldt Bay Middle Channel (HBMC) Bridge, one of the six PEER testbeds. The probabilistic performance assessment of the bridge system is broken down into four steps: (1) probabilistic seismic hazard analysis (PSHA), (2) probabilistic seismic demand analysis (PSDA), (3) probabilistic capacity analysis (or fragility analysis), and (4) reliability analysis. PSHA computes the seismic hazard for the bridge site based on the ground motion intensity measure (*IM*) defined as the 5 percent undamped elastic spectral acceleration at the low amplitude vibration predominant period of the bridge ground system. Based on the results of PSHA and the local seismology, a set of 51 actual ground motion time histories is developed to represent three different hazard levels, namely 50%, 10%, and 2% probability of exceedance in 50 years (return periods of 72, 475, and 2,475 years, respectively). A two-dimensional advanced nonlinear finite element model of the bridge-foundation-soil system is developed in OpenSees and subjected to each of the 51 ground motion time histories. Three potential failure mechanisms are considered: flexural failure of lap spliced piers, failure of shear keys, and unseating. For each failure mechanism, five limit-states with associated *EDP* (Engineering Demand Parameter) are defined. Simulation results of each *EDP* are analyzed statistically to estimate the probability distribution of the *EDP* conditioned on *IM*. PSDA computes the seismic demand hazard for each *EDP* by convolving the conditional probability distribution of the *EDP* given *IM* with the seismic hazard curve. Experimental data on the various limit-states characterizing the failure mechanisms considered are collected and analyzed. Using this experimental data in conjunction with mechanistic predictive capacity models, fragility curves are derived to predict the conditional probability of exceeding a certain limit-state given the *EDP*. The seismic reliability analysis step computes the mean annual rate/frequency of exceeding a system-level limit-state by convolving its fragility curve with the corresponding demand hazard curve. The computational results obtained for the HBMC Bridge indicate that the most critical damage-states are the initiation (return period from 15 to 20 years) and full development (return period from 19 to 39 years) of the shear keys failure mechanism, followed by flexural yielding in the lap-spliced region at the base of the bridge piers (return period of 40 years). Unseating is found to be very unlikely, due to the typical deformation pattern of the bridge ground system during an earthquake. In the last step of the PEER PBEE methodology, called loss analysis, the probabilistic performance assessment results presented herein will be propagated further to decision variables of greatest interest to stakeholders, such as downtime, loss of functionality and repair cost.

ACKNOWLEDGEMENTS

This work was supported primarily by the Earthquake Engineering Research Centers Program of the National Science Foundation, under Award Number EEC-9701568 through the Pacific Earthquake Engineering Research Center (PEER). Any opinions, findings and conclusions or recommendations expressed in this material are those of the author(s) and do not necessarily reflect those of the National Science Foundation. This support is gratefully acknowledged. The authors wish to thank Mr. Patrick Hipley, Dr. Cliff Roblee, Dr. Charles Sikorsky, Mr. Mark Yashinsky, and Mr. Tom Shantz of Caltrans for providing all the requested information regarding the initial design and retrofits of the Humboldt Bay Middle Channel Bridge. Prof. Greg Fenves, Dr. Frank McKenna, and Mr. Michael Scott (U.C. Berkeley), Prof. Jacobo Bielak (Carnegie Mellon University), and Prof. Jose Restrepo (U.C. San Diego) helped with the geotechnical and structural modeling and analysis aspects of this work. Their help is gratefully acknowledged. The authors also want to thank Dr. Paul Somerville (URS Corporation), Prof. C. Allin Cornell (Stanford Univ.) and Prof. Mark Eberhard (Univ. of Washington) for insightful discussions on probabilistic seismic hazard analysis, probabilistic performance assessment, and fragility analysis.

REFERENCES

1. Porter, K.A. "An overview of PEER's performance-based earthquake engineering methodology." *Proc. Ninth International Conference on Applications of Statistics and Probability in Civil Engineering (ICASP9)*, Volume 2, pp. 973-980, San Francisco, CA, USA, July 6-9, 2003.
2. Cornell, C. A., Krawinkler, H. "Progress and challenges in seismic performance assessment." PEER Center News 2000; 3(2).
3. Cornell, C.A. "Engineering seismic risk analysis." Bull. Seism. Soc. Am., 1968, 58: 1583-1606.
4. Abrahamson, N.A., Silva, W.J. "Empirical response spectral attenuation relations for shallow crustal earthquake." *Seismological Research Letter*, 1997, 68(1): 94-109.
5. Campbell, K.W. "Empirical near-source attenuation relationships for horizontal components of peak ground acceleration, peak ground velocity, and pseudo-absolute acceleration response spectral." *Seismological Research Letter*, 1997, 68(1): 154-19.
6. Jalayer, F., Cornell, C. A. "Alternate nonlinear demand estimation methods in probability-based seismic assessment." *Manuscript*, Stanford University, January 2002.
7. Luco, N., Cornell, C. A. "Structure-specific scalar intensity measures for near-source and ordinary earthquake ground motions." Earthquake Spectra, in press, 2004.
8. Gardoni, P., Der Kiureghian, A., Mosalam, K.M. "Probabilistic capacity models and fragility estimates for RC columns based on experimental observations." *J. of Eng. Mech.*, ASCE, 2002, 128(10): 1024-1038.
9. Somerville, P., Collins, N. "Ground motion time histories for the Humboldt Bay Bridge." *Report of the PEER Performance Based Earthquake Engineering Methodology Testbed Program*, 2002, Pacific Earthquake Engineering Research Center, University of California at Berkeley, Berkeley, CA.
10. Frankel, A., et al. "USGS national seismic maps: documentation." USGS Open File Report 96-532, 1996.
11. Geomatrix Consultants. "Seismic ground motion study for Humboldt Bay bridges on Route 255, Humboldt Country, California." Contract # 59N772. Rep. prepared for Caltrans Div. of Structures, 1994.
12. Pacific Gas & Electric Company. "Appendix A to Section 2.5 Humboldt Bay ISFSI Site Safety Analysis Report." 2001.
13. Somerville, P.G., Smith, N.F., Graves, R.W., Abrahamson, N.A. "Modification of empirical strong ground motion attenuation relations to include the amplitude and duration effects of rupture directivity." *Seismological Research Letters*, 1997, 68: 199-222.
14. Conte, J.P., Elgamal, A., Yang, Z., Zhang, Y., Acero, G., F. Seible "Nonlinear seismic analysis of a bridge ground system." (CD-ROM), *Proceedings of the 15th ASCE Engineering Mechanics Conference*, Columbia University, New York, June 2-5, 2002.
15. McKenna, F., Fenves, G.L. "The OpenSees command language manual, version 1.2." 2001, Pacific Earthquake Engineering Research Center, University of California at Berkeley.
16. Spacone, E., Filippou, F.C., Taucer, F.F. "Fibre beam-column model for non-linear analysis of R/C frames: Part I. Formulation." *Earthquake Engineering and Structural Dynamics*, 1996, 25 (7), 711-725.
17. Elgamal, A., Yang, Z., Parra, E., Ragheb, A. "Modeling of cyclic mobility in saturated cohesionless soils." *International Journal of Plasticity*, 2003, 19(6), 883-905.
18. Zhang, Y., Yang, Z., Bielak, J., Conte, J.P., Elgamal, A. "Treatment of seismic input and boundary conditions in nonlinear seismic analysis of a bridge ground system." *Proceedings of the16th ASCE Engineering Mechanics Conference*, University of Washington, Seattle, July 16-18, 2003.
19. Schnabel, P.B., Lysmer, J., Seed, H.B. "SHAKE: a computer program for earthquake response analysis of horizontally layered sites." *Report No. EERC 72-12*, Earthquake Engineering Research Center, University of California at Berkeley, CA, 1972.
20. Silva, W., Turcotte, T., King, J., Moriwaki, Y. "Soil response to earthquake ground motion." Research Project RP2556-07, Final Report, Woodward-Clyde Consultants, September 1986.
21. Hose, Y. D., Seible, F. "Performance evaluation detabase for concrete bridge components and systems under simulated seismic loads." Pacific Earthquake Eng. Res. Center, Report PEER 1999/11, Nov. 1999.
22. Bozorgzadeh, A., Megally, S., Restrepo, J.I., Ashford, S.A. "Seismic response and capacity evaluation of exterior sacrificial shear keys of bridge abutments." Proceedings of the 13th World Conference on Earthquake Engineering, Vancouver, B. C., Canada. Paper no. 528, 2004
23. Megally, S. H., Silva, P. F., Seible, F. "Seismic response of sacrificial shear keys in bridge abutments." University of California, San Diego, Report SSRP - 2001/23.
24. Priestley, M. J. N., Seible, F. "Seismic assessment and retrofit of bridges." University of California, San Diego, SSRP Report 91/03, July 1991: 84-149.
25. Melek, M., Wallace, J. W., and Conte, J. P. "Experimental assessment of columns with short lap splices subjected to cyclic loads." Pacific Earthquake Engineering Research Center, Report PEER 2003/04, College of Engineering, University of California, Berkeley, April 2003.